Power System Technology
ISSN:1000-3673

Received: 06-06-2024 Revised: 15-07-2024 Accepted: 28-08-2024

A Design of SEPIC Converter for Powering the Wireless Sensor Nodes in a Bridge Monitoring Setup Using a Piezoelectric Energy Harvester

Muhammad Kamran[1], Imtiaz Rasool[1], Faiz Ullah[3], Muhammad Wasimuddin[1], Muhammad Noman Khan[1,2], Nadir Ali Khan[1]

[1]Department of Electronics, University of Peshawar, Peshawar, Pakistan

[2]Department of Journalism and Mass Communication, University of Peshawar, Peshawar, Pakistan

[3]Department of Electronics, Islamia College University, Peshawar, Pakistan

Email addresses:

kamranmu@uop.edu.pk

imtiazrasoolkhan@uop.edu.pk

faiz@icp.edu.pk

wasimuddin@uop.edu.pk

noman@uop.edu.pk

nakhan@uop.edu.pk

Corresponding Author:

Muhammad Kamran

Email: kamranmu@uop.edu.pk

Postal Address: Assistant Professor, Department of Electronics, University of Peshawar, Peshawar, KP, Pakistan.

Abstract:- In this paper, a DC-DC converter for powering the wireless sensor node in a bridge monitoring system is presented. The continuous monitoring of a bridge is essential to keep track of its strength and estimate its lifetime, because an old bridge may be a threat to hundreds of human lives. Therefore, in most countries the bridges are regularly monitored using electronic sensors and data from all these sensors is then collected to a central point, which is in most cases a personal computer or cloud system. However, the major problem in this setup is sending and receiving the data of all the sensors from distant locations to a single point. The reason is that sometimes the length of the bridge is more than one kilometre and even up to five kilometres. In this regard, different methods have been suggested to resolve this problem, but one of the efficient ways is to use the Wireless Sensor Network (WSN) to share data of all the sensors because a typical WSN node is already equipped with some built-in sensors and other sensors can also be easily interfaced with it. The WSN nodes require a 3.3V DC supply for their operation, which can be provided by the small rechargeable batteries, but the main challenge in

Power System Technology
ISSN:1000-3673
Received: 06-06-2024 Revised: 15-07-2024 Accepted: 28-08-2024

this scenario is the charging of the batteries. In a bridge monitoring system, this battery charging can easily be done by converting the bridge vibrations to electric power by using a piezoelectric energy harvester (PEH). The output power of a PEH greatly depends upon the mechanical stress applied to its surface. A typical PEH will produce a voltage from 1 volt up to 5 volts and its output current is in milli amperes (mA). Now to get more power from these energy harvesters, multiple PEHs can be connected in series and parallel to produce more electric power. An array of 25 PEH can easily provide power to a single WSN mote and charge its battery. But the problem is, that, the WSN node requires 3.3VDC, while the output voltage of the PEH array will be continuously varying between 2V and 20V depending upon the intensity of the bridge vibrations. To solve this issue an improved DC-DC SEPIC converter has been designed and tested in this research. The results show that the designed converter is capable of providing power to the WSN node and charging its battery.

Keywords: *DC-DC SEPIC converter, Wireless Sensor Network, Bridge Monitoring, Piezo Electric Energy Harvester*

1 Introduction

In recent years, power electronics circuits have been employed in many commercial products and industrial control systems, i.e., electric vehicles (EVs), power inverters, motor speed controllers and voltage conversion from one level to another [1][2]. The reason is their high efficiency and simple circuitry. The types of different converter circuits are DC-DC, DC-AC, AC-DC and AC-AC power converters [3]. Different topologies have been adopted for these converters to fulfil the requirements of the mentioned applications [4]. The scope of this research is a DC-DC converter for powering the WSN nodes. There are several configurations of DC-DC converters, like buck, boost, buck-boost and SEPIC converters. A buck converter converts a high-voltage DC into a lower voltage, while a boost will do its opposite function. The buck-boost converter can work as both a buck and boost converter, but the problem is that its output is inverted. The best option in this scenario is a SEPIC converter, which increases or decreases the DC voltage applied at its input with a non-inverted output. In this research work, the power to the WSN nodes has been provided by an array of PEH, which gives a DC voltage of 2 to 20V according to the vibration intensity of the vehicles passing over the bridge. So we need a DC-DC converter that can convert a wide range of voltage (2V to 20V) to a fixed output voltage of 3.3V, which is required by a WSN node and charging its battery [5][6]. It means, that it should work as both the buck and boost with non-inverted output voltage. Therefore, the SEPIC converter is the best choice for this application [7]. The architecture of the overall system is given in Figure 1. The PEH array is composed of a 5 by 5 harvester, which produces a voltage between 2 and 20 volts depending upon the pressure exerted by the vehicles [8]. The output of the piezoelectric array is an alternating current (AC) voltage. Since the WSN node requires a DC voltage, therefore, a diode bridge has been used for converting AC into DC

Power System Technology
ISSN:1000-3673
Received: 06-06-2024 Revised: 15-07-2024 Accepted: 28-08-2024

voltage. The SEPIC converter is a closed-loop DC-DC SEPIC converter, which will provide a stable 3.3VDC for a wide range of input voltage. The output of the SEPIC converter will be used to charge the battery as well as provide power to the WSN node and all the sensors connected with it.

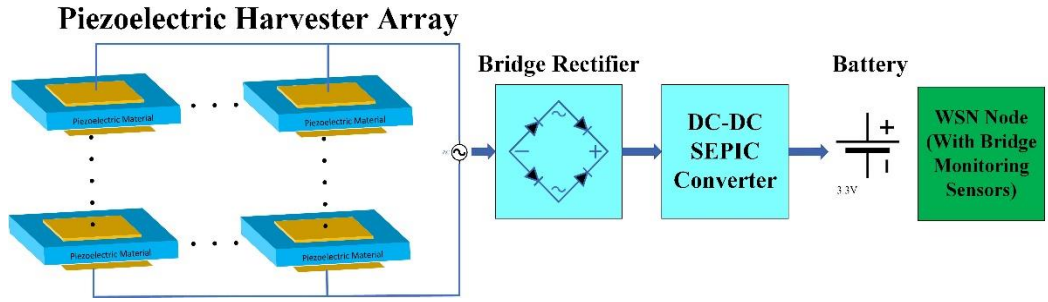

Figure 1 (Overall Block Diagram)

2 Bridge monitoring and Wireless Sensor Network

2.1 Bridge Monitoring

In a bridge monitoring system, different parameters of the bridge are monitored using adequate sensors. The important parameters and the sensors used for this purpose are given in Table 1. These sensors are mounted on the bridge at a suitable distance and a set of all these sensors is connected to a WSN node. The common WSN nodes have one or two sensors onboard, while several other analog and digital sensors can be interfaced using its ports. The WSN nodes fixed on the bridge at different locations communicate with each other and pass on the collected data from one end of the bridge to the other end [9]. In other words, all the WSN nodes form a wireless network to sense and share different bridge parameters to measure its strength and the remaining lifetime of the bridge [10].

Table 1(Bridge parameters to be monitored with required sensors)

Parameters to be monitored	**Type of Sensors**
Girder Displacement	ADXL345, A 3D Accelerometer
Towers Displacement	Laser-based drift monitor
Strain/ Stress of the main Girder	EFPI Fiber-Optic strain sensor
Temperature field of the main Girder	DHT22 (Precise digital Temperature Sensor)
Cable Tension and Vibration	VS-97 Accelerometer

Power System Technology
ISSN:1000-3673
Received: 06-06-2024 Revised: 15-07-2024 Accepted: 28-08-2024

2.2 Wireless Sensor Network

A Wireless Sensor Network (WSN) is composed of many communicating devices with sensing capabilities called sensor nodes (or motes) [11]. A typical WSN network includes 10s to 100s of WSN motes and each mote contains a microprocessor, two or more sensors and a radio transceiver. The radio and network technologies used in the motes can be used to create a wireless network, where each WSN node can acquire environmental or other information through the sensors and can share it with other motes. This type of network provides a more flexible arrangement and lesser maintenance costs. Each node has a CPU, a power supply, commonly a battery and a radio transceiver with an internal antenna or linking to an external antenna for communication [12][13][14].

The wireless sensor network contains multiple sensor nodes and one base station. After collecting the data from all the sensors, the base station sends all the acquired data to a cloud system through the Internet for storage and further analysis. These sensors are connected with the WSN mote through its extension ports. The embedded processor inside the WSN mote reads the bridge parameters through these sensors. A typical WSN network for such applications is given in Figure 2 [15].

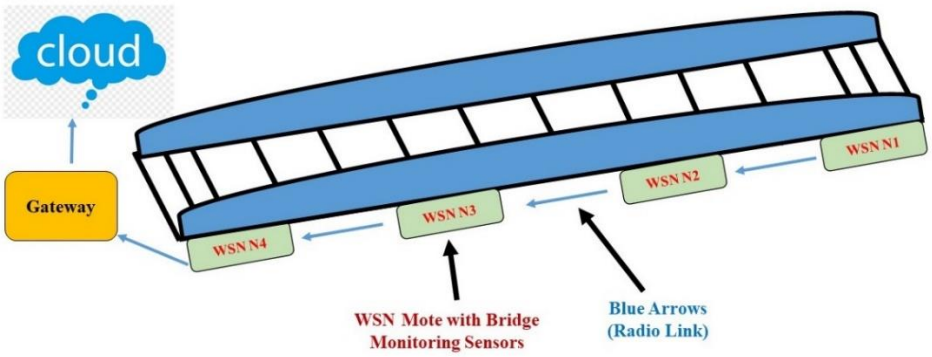

Figure 2 (WSN Mote and Sensors setup on a bridge)

The multiple WSN nodes are fixed on the bridge at a distance easily covered by the radio signals of the WSN mote. Each WSN node in Figure 2 has a WSN mote along with sensors for bridge parameters monitoring. They have been placed at a distance easily covered by the communication range of an individual mote. The WSN nodes require electrical energy to perform their functions like sensing and communication. One solution is to use battery cells for this purpose, but the issue is that they have a limited lifetime and must be replaced before fully discharged to avoid any data loss. But this solution is not feasible due to the high cost of new batteries and their short replacement period. The architecture of a typical WSN network is given in Figure 3.

Power System Technology
ISSN:1000-3673
Received: 06-06-2024 Revised: 15-07-2024 Accepted: 28-08-2024

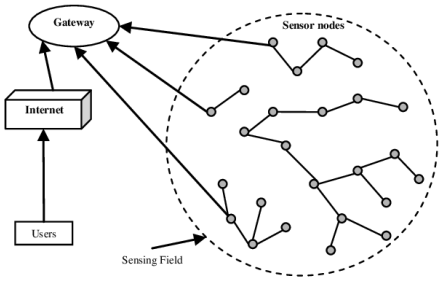

Figure 3 (A typical WSN Netwrok Architecture)

2.2.1 WSN Mote used

Each sensor node used in the proposed bridge monitoring system is a TelosB WSN mote, which contains a powerful microcontroller, 2.4GHz Radio, multiple channels of analog to digital converter and Extention ports for interfacing the external sensors. In this experimental setup, four TelosB WSN motes were used, the front side is given in Figure 4.

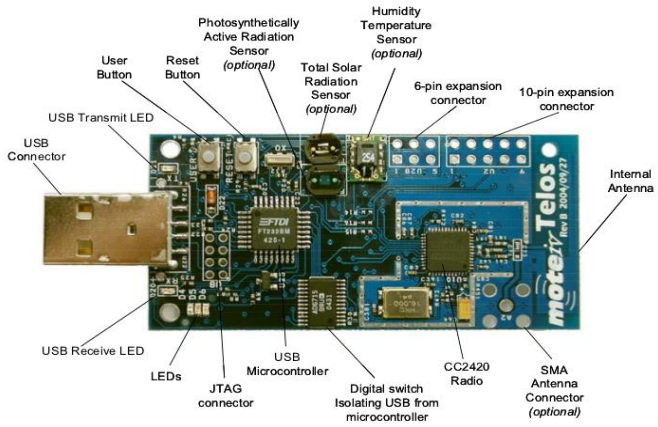

Figure 4 (WSN Mote TelosB)

The essential feature of a WSN mote is, that, it should consume ultra-low power to work for a long period with a single charge of the battery. Due to this reason, many researchers have used this WSN mote in their systems and we have also selected it for the bridge monitoring system, as it consumes a very small amount of electrical energy [9].

3 Piezoelectric Energy Harvesting

3.1 The Piezoelectric effect

Several natural substances, including quartz, Rochelle salt, topaz, tourmaline, and Berlinite (which are physically identical to quartz), exhibit the piezoelectric effect [16]. Four categories of ceramics, composites, polymers, and single crystals can be used to manufacture piezoelectric materials for energy harvesting [17]. The piezoelectric effect describes how certain materials

Power System Technology
ISSN:1000-3673
Received: 06-06-2024 Revised: 15-07-2024 Accepted: 28-08-2024

can generate an electric charge in response to mechanical stress. The piezoelectric effect is reversible, as materials that give the direct piezoelectric effect, which causes electricity to be generated when stress is applied, can also exhibit the reverse piezoelectric effect. Which causes stress to be generated when an electric field is applied [18]. The positive and negative charge carriers within a piezoelectric material shift in response to mechanical stress, creating an external electrical field [19]. When the electrical field is reversed, the piezoelectric material is compressed or stretched. The creation and detection of sound, high-voltage generation, electronic frequency generation, microbalances, and ultra-fine optical assembly focusing are just a few of the applications where the piezoelectric effect is useful. Many atomic-resolution scientific tools, including scanning probe microscopes (STM, AFM, etc.), are built on this phenomenon [20]. A more commonplace application of the piezoelectric effect is as an ignition source in cigarette lighters. The piezoelectric effect's working operation is presented in Figure 5 [21]. When the voltage is zero in the normal condition, which is when no external force is applied. Nevertheless, voltage is produced when tension or compression is applied [22][23].

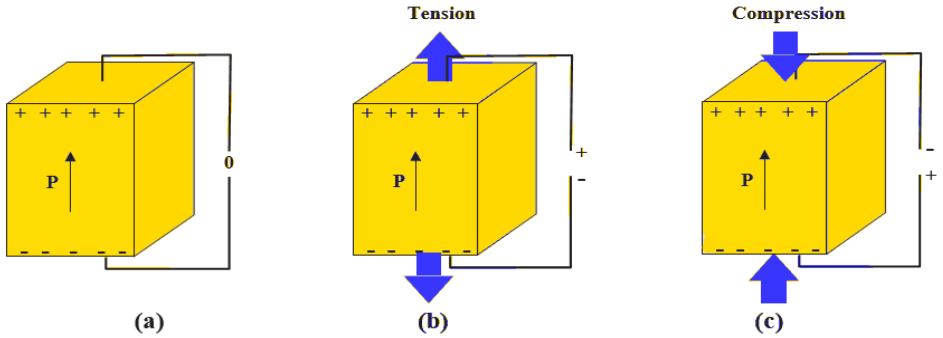

Figure 5 (Working principle of piezoelectric effect (a) zero stress; (b) tension; and (c) compression [21])

The relations for the piezoelectric materials are given below (IEEE Standard, 1987):

(i) Direct Piezoelectric Effect:

$$D_i = e_{ij}^{\sigma} + d_{im}^{d}\sigma_m \quad (1)$$

(ii) Reverse Piezoelectric Effect:

$$\varepsilon_k = d_{jk}^{c}E_j + s_{km}^{e}\sigma_m \quad (2)$$

(iii) It can also be written as:

Power System Technology
ISSN:1000-3673
Received: 06-06-2024 Revised: 15-07-2024 Accepted: 28-08-2024

$$\begin{bmatrix} D \\ \varepsilon \end{bmatrix} = \begin{bmatrix} e^{\sigma} & d^{d} \\ d^{c} & s^{E} \end{bmatrix} \begin{bmatrix} E \\ \sigma \end{bmatrix} \quad (3)$$

In the above expressions:
"D = electric displacement vector of the size (3×1) (Coulomb/m²), ε vector (6×1) is the strain
E vector (3×1) (Volt/m) = the applied electric field, σ^{m} and vector (6×1) (N/m²) is a stress
The piezoelectric constants are the dielectric permittivity e_{ij}^{σ} of size (3×3) (Farad/m)
The piezoelectric coefficients d_{im}^{d} (3×6) and d_{jk}^{c} (6×3) (Coulomb/N or m/Volt)
and the elastic compliance s_{km}^{e} of size (6×6)(m²/N)
The piezoelectric coefficient d_{jk}^{c} (m/Volt) defines strain per unit field at constant stress
and d_{im}^{σ} (Coulomb/N) defines electric displacement per unit stress at a constant electric field" [3][23].

3.2 Simulink model of the piezo bender energy harvester

To realize the overall process of energy harvesting from the piezoelectric harvesters, a model of piezo bender has been designed and simulated in the MATLAB/ Simulink environment [24][25]. The model consists of a vibration source, a piezo bender, a bridge rectifier, and a DC-DC converter. The piezo bender harvests energy from a vibration source. The energy harvested from the piezo bender is used to charge a battery and provide power to a load. The model is given in Figure 6.

Piezoelectric benders are flexible beams having a natural fundamental frequency of oscillation from a mechanical standpoint. A piezo bender generates the most power when it oscillates at this resonant frequency. Since the source's frequency is closer to the resonant frequency, it generates nearly the maximum amount of power from this energy harvester [26]. The signal generated by the vibration source is a "chirp" signal, whose frequency increases and decreases.

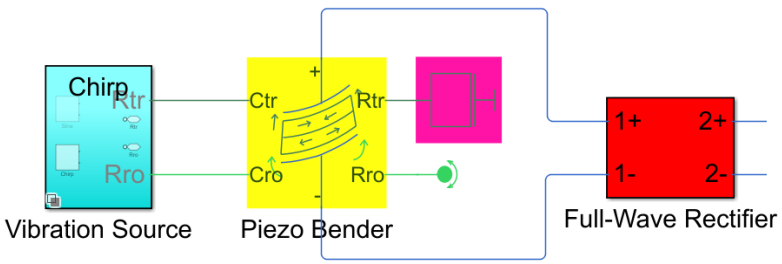

Figure 6 (Simulink Experimental setup of piezo Bender to get voltage and power [24]*)*

Power System Technology
ISSN:1000-3673
Received: 06-06-2024 Revised: 15-07-2024 Accepted: 28-08-2024

The left side of the piezo bender is clamped to a vibrating item, which forces the motion. An extra mass is allied to the right side of the piezo bender [24]. The right end's motion is not synchronized with the left end due to the piezo bender's elasticity, mass, and inertia. The deformations produce a charge and voltage across the piezo bender's electrical terminals, which are gathered as electricity. The piezo bender generates AC power, which is converted to DC power by a full-wave rectifier. It has four diodes and a filter capacitor that smooths the DC voltage. The energy harvester starts by charging a battery. The energy harvester and the battery are then both powered up at the same time.

The buck converter controls the voltage to deliver the highest amount of power to the load while maintaining unidirectional power transfer. In this case, the converter is controlled in an open loop by a pulse generator with a fixed switching frequency and duty cycle. You can develop a more sophisticated closed-loop controller to optimize the transmission of power and improve the performance of the energy harvester under varied settings if the vibration source does not have a constant frequency or contains harmonics [27].

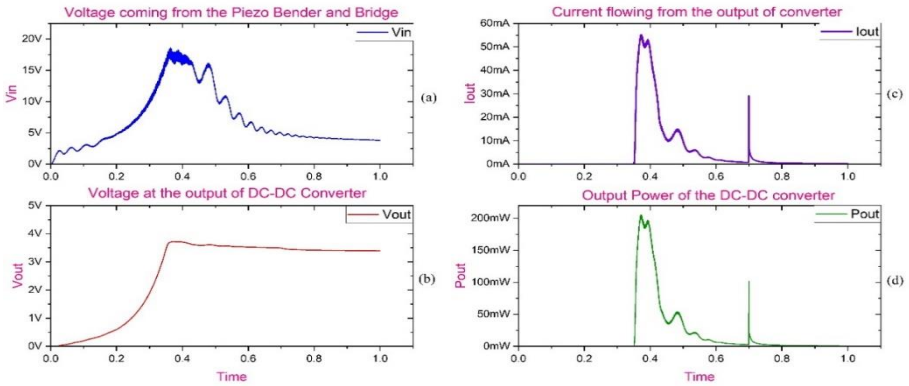

Figure 7 (a) voltage from the piezo bender, (b) output of converter (c) output current and (d) output power

Figure 7(a) shows the output of the piezo bender after passing through the bridge rectifier. There are fluctuations in the output voltage due to the variations in the vibration's frequency. In Figure 7(b), the output of the converter is given. The output of the converter is initially increasing and after reaching the required value, it is almost constant. When the vibration frequency approaches the resonant frequency, it generates maximum power [28]. In Figure 7(c), the output current flowing toward the battery and load is given, while in Figure 7(d), the power dissipated in charging the battery and load is given.

3.3 Placement of the PEHs on the bridge to harvest Energy from the bridge traffic

There are two mechanisms of energy harvesting from the PEH. First, when, huge vehicles pass on the bridge, there would be high-intensity vibrations on the bridge. These vibrations will provide mechanical stress to the PEHs and as a result, a small amount of electric energy will

Power System Technology
ISSN:1000-3673
Received: 06-06-2024 Revised: 15-07-2024 Accepted: 28-08-2024

be generated [29]. Secondly, some PEHs have also been used on the surface of the bridge road, so the passing of the vehicles will provide mechanical stress to them and they will produce energy. To get more energy, multiple PEHs have been used in series and parallel configurations [30].

Figure 8 (Placement of piezoelectric energy harvesters on the bridge)

In this experimental setup, the PEHs have been placed on the road in such a way, that the passing of the vehicle on the bridge will provide them with mechanical stress, see Figure 8. This mechanical stress will become the means of generating energy from them [29]. A 3.3V high-capacity battery is connected to each WSN mote and its sensors. The energy source for charging the battery is the electrical power generated by the PEHs array. In this experimental setup, an array of 25 PEHs is used in series and parallel configurations to get more power. The output energy from the PEHs array is an alternating current and its strength is continuously varying according to the strength of vibrations on the bridge [31]. Therefore, first, it was converted into DC voltage using a bridge rectifier and then a DC-DC SEPIC converter was used to provide a stable 3.3V ripple-free electrical energy to each WSN node. The overall arrangement of the WSN nodes and piezoelectric energy harvester on the bridge is shown in Figure 2 in Section 2.2. The DC voltage at the output of the bridge rectifier varies continuously due to the variations in the intensity of bridge vibrations. The result shows, that the amplitude of DC voltage varied between 2V and 20V at the output of the rectifier.

Power System Technology
ISSN:1000-3673
Received: 06-06-2024 Revised: 15-07-2024 Accepted: 28-08-2024

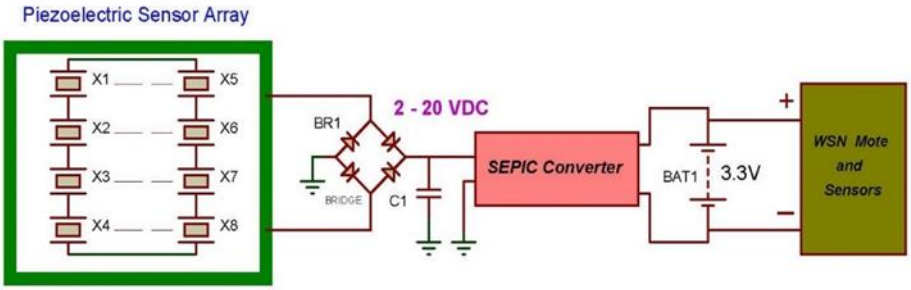

Figure 9 (The overall design of Energy harvester)

The overall schematic of the energy harvesters, bridge rectifier, SEPIC converter and WSN node is given in Figure 9. The WSN nodes used in this experimental setup are Telosb. These motes require a 3.3VDC supply and the same voltage is also needed for charging the battery connected with the WSN mote to provide power in the absence of traffic on the bridge. In this regard, we need an electronic circuit, which can convert a wide voltage range into a fixed 3.3V. When the amplitude of DC voltage at the output of the rectifier is less than 3.3V, then it should work as a boost converter, while in another case, when the voltage is greater than 3.3V, then it should work as a buck converter. So the solution is a SEPIC converter, which stands for a Single-ended primary inductor converter [32]. For better performance of the SEPIC converter, it is equipped with an intelligent controller to keep the output voltage constant.

4 Design and analysis of the SEPIC Converter

4.1 Basic SEPIC Converter

A DC-DC SEPIC converter is a type of DC-DC converter that can step up or step down the DC voltage [7]. SEPIC stands for Single-Ended Primary Inductance Converter. This type of converter uses a capacitor, an inductor, and a switch to regulate the output voltage. The SEPIC converter has a few advantages over other types of DC-DC converters, including efficient power transfer, the ability to handle a wide range of input voltages, and low output ripple. As a result, SEPIC converters are commonly used in applications such as LED lighting, battery-powered devices, and automotive electronics.

4.1.1 Analysis of basic SEPIC Converter

The successful design and control of DC-DC converters involve a series of mathematical steps documented in [33][34]. To achieve optimal performance, various cost, efficiency, size, and component selection aspects must be carefully examined. Two fundamental principles of circuit analysis are used to determine the steady-state voltage and current waveforms of a DC-DC converter [35][34]. According to the inductor volt-second balance principle [36], the

Power System Technology
ISSN:1000-3673
Received: 06-06-2024 Revised: 15-07-2024 Accepted: 28-08-2024

average or DC value of the voltage applied across an ideal inductor must be zero. Likewise, based on the law of capacitor amp-second balance, the average current passing through an ideal capacitor must be zero. By averaging inductor current and capacitor voltage across one switching period and equating the results to zero, the voltages and currents of DC-DC converters can be obtained.

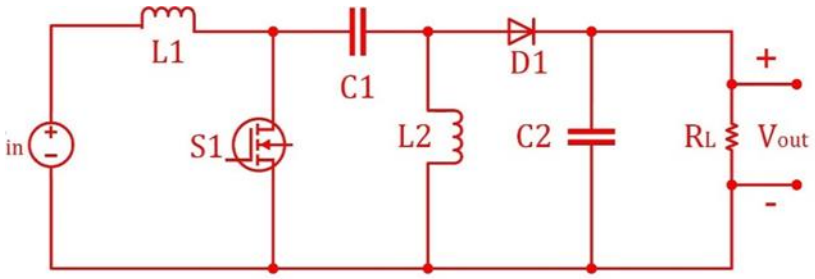

Figure 10 (Simplified circuit diagram of a SEPIC converter)

The voltages and current through the different components of a SEPIC converter are shown in Figure 11. The basic rules and law of circuit analysis will be applied to derive all the unknown parameters as shown in figure 11.

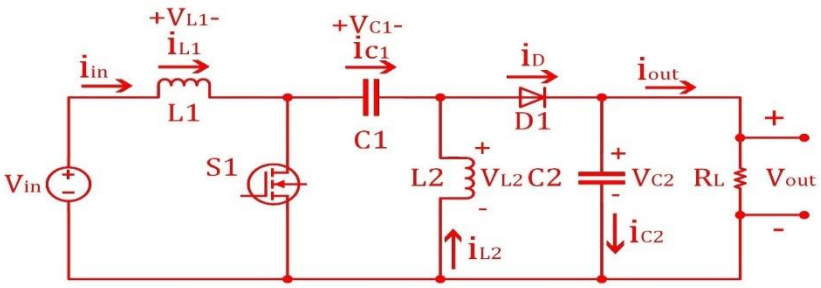

Figure 11 (Voltage polarities and current directions)

Inductor currents and capacitor voltages contain DC components and voltage ripples at the switching frequency along with its harmonics. In both cases, the ripple magnitude is small compared with the dc component and can be ignored. Under normal operation, the circuit is in a continuous conduction state i.e. Inductors currents iL1 and iL2 are always greater than zero [33]. When the switch is closed for DT (T= ton + toff) seconds, capacitor C1 is charged to Vin, energy is stored in L1 from the Vin and in L2 from C1, and the diode is reverse biased and like an open, as shown in figure 12.

Power System Technology
ISSN:1000-3673
Received: 06-06-2024 Revised: 15-07-2024 Accepted: 28-08-2024

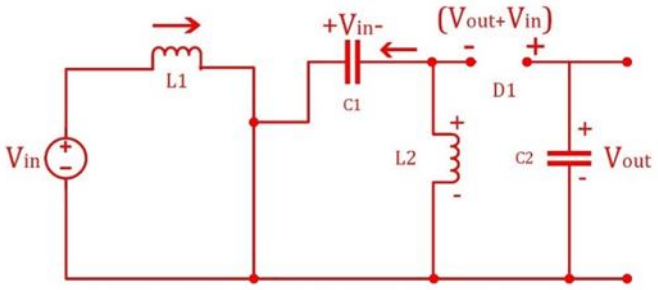

Figure 12 (Switch close state)

When the switch is open for D'T seconds as shown in Figure 13, the diode is forward biased and the iL1 current continues to flow through C1 and D1 and into C2. Both C2 and C1 get recharged so that they can provide current to the load and charge L2.

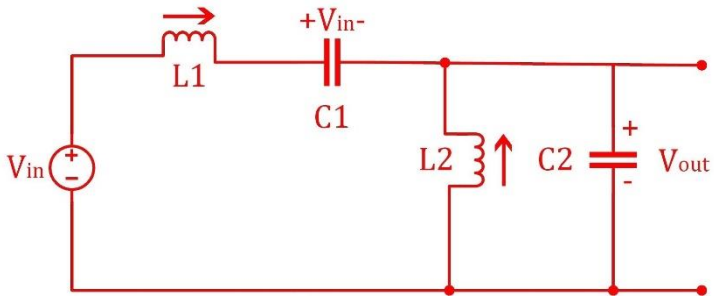

Figure 13 (switch open state)

The first relationship can be found by applying KVL around the loop formed by Vin, L1, C1, and L2, and recognizing that the average voltages across inductors L1 and L2 are zero, yields

$$V_{in} = V_{L1} + V_{L2} + V_{C1}$$

$$V_{C1} = V_{in} \tag{4}$$

We will derive this relationship described by equation (6) using the inductor's volt-second balance law. Because of the steady-state inductor principle, mentioned above, the average voltage across L1 and L2 is zero. Since VL1 and VL2 have two states, the switch-on state and the switch-off state. The average value of V_{L1} and V_{L2} is

$$\langle \boldsymbol{V}_{L1} \rangle, \langle \boldsymbol{V}_{L2} \rangle = 0$$

(5)

Power System Technology
ISSN:1000-3673
Received: 06-06-2024 Revised: 15-07-2024 Accepted: 28-08-2024

Applying the switch on state DT and switch off state D'T for inductor L1 we have

$$\langle V_{L1} \rangle = DV_{in} + D'(V_{in} - V_{out} - V_{C1}) \quad (6)$$

$$DV_{in} + (1-D)(V_{in} - V_{out} - V_{C1}) = 0 \quad (7)$$

$$V_{in} - V_{out} - V_{C1} + DV_{out} + DV_{C1} = 0 \quad (8)$$

$$V_{in} - V_{out}(1-D) - V_{C1}(1-D) = 0$$

$$V_{in} - V_{out}D' - V_{C1}D' = 0$$

$$D'V_{C1} = V_{in} - V_{out}D'$$

$$V_{C1} = \frac{V_{in}}{D'} - V_{out} \quad (9)$$

Now apply switch-on state DT and switch-off state D'T for inductor L2

$$\langle V_{L2} \rangle = DV_{C1} - D'V_{out} = 0 \quad (10)$$

$$V_{C1} = \frac{D'V_{out}}{D} \quad (11)$$

Substitute (9) and (11) yields the voltage transfer function of a SEPIC converter

$$\frac{V_{in}}{D'} - V_{out} = \frac{D'V_{out}}{D}$$

$$\frac{V_{in}}{D'} = \frac{D'V_{out}}{D} + V_{out}$$

$$D'V_{out} + DV_{out} = \frac{V_{in}D}{D'}$$

$$V_{out} = \frac{V_{in}D}{D'} \quad (12)$$

$$\frac{V_{out}}{V_{in}} = \frac{D}{D'} = M(D) \quad (13)$$

From (13) it is clear that the converter is in a buck or step-down mode for D < 0.5, and in boost or step-up mode for D > 0.5. In terms of input and output currents

Power System Technology
ISSN:1000-3673
Received: 06-06-2024 Revised: 15-07-2024 Accepted: 28-08-2024

$$\frac{I_{out}}{I_{in}} = \frac{D'}{D} = M(D) \tag{14}$$

Substituting (12) into (11) yields

$$V_{C1} = \left(\frac{D'}{D}\right)\left(\frac{V_{in}D}{D'}\right) = V_{in}$$

$$V_{C1} = V_{in} \tag{15}$$

Which is the same result obtained in (4) by applying KVL on the circuit given in Figure 8.

The second important relationship can be found by applying KCL on the circuit of Figure 8 at the top node of L2. Since the average currents in C1 and C2 are both zero, thus

$$I_{C1} = I_{L2} + I_D$$

Where $I_D = I_{out} + I_{C2}$ yields

$$I_{L2} = I_D = I_{out} \tag{16}$$

Now we will derive this relationship described by (16) using charge balance.

Applying charge balance on $< I_{C1} > and < I_{C2} >$ and with switch on state DT and switch off state D'T we have

$$\langle I_{C1} \rangle = -DI_{L2} + D'I_{L1} = 0 \tag{17}$$

$$D'I_{L1} = DI_{L2}$$

$$I_{L1} = \frac{D}{D'} I_{L2} \tag{18}$$

$$\langle I_{C2} \rangle = -\frac{DV_{out}}{R} + D'\left(I_{L1} + I_{L2} - \frac{V_{out}}{R}\right) = 0 \tag{19}$$

$$\frac{-DV_{out}}{R} + D'(I_{L1} + I_{L2}) - \frac{(1-D)V_{out}}{R} = 0$$

$$D'(I_{L1} + I_{L2}) - \frac{V_{out}}{R} = 0$$

Power System Technology
ISSN:1000-3673
Received: 06-06-2024 Revised: 15-07-2024 Accepted: 28-08-2024

$$\frac{V_{out}}{R} = D'\left(I_{L1} + I_{L2}\right)$$

$$I_{L1} = \frac{V_{ou}t}{D'R} - I_{L2} \tag{20}$$

Substitute (20) into (18) yields

$$\frac{D}{D'} I_{L2} = \frac{V_{out}}{D'R} - I_{L2}$$

$$I_{L2}\left(\frac{1}{D'}\right) = \frac{V_{out}}{D'R}$$

$$I_{L2} = \frac{V_{out}}{R} = I_{out} = I_D$$

$$I_{L2} = I_{out} = I_D \tag{21}$$

Which is the same result obtained in (16) by applying KCL on Fig. 3

$$I_{L2} = \frac{V_{out}}{R} = \frac{V_{in}D}{RD'} \tag{22}$$

$$I_{L1} = I_{L2}\left(\frac{D}{D'}\right) = \frac{V_{in}D}{RD'}\left(\frac{D}{D'}\right) = \frac{V_{in}}{R}\left(\frac{D^2}{D'^2}\right) \tag{23}$$

Equations (22) and (23) are used to find inductor L1 and inductor L2 currents respectively.

These derived equations can be used to find the voltages and currents across and through all the elements of a SEPIC converter.

4.2 Selection of different parameters and components

4.2.1 Duty Cycle

The amount of voltage that SEPIC converters can regulate depends on the Duty Cycle and the parasitic elements in the circuit. To find the duty cycle for a SEPIC converter let us rewrite (12)

$$V_{out} = \frac{V_{in}D}{D'} \tag{24}$$

Substitute $D' = 1 - D$ into (24) we have

Power System Technology
ISSN:1000-3673
Received: 06-06-2024 Revised: 15-07-2024 Accepted: 28-08-2024

$$V_{out} = \frac{V_{in} D}{1-D}$$

$$V_{out}(1-D) = V_{in} D$$

$$V_{out} = D(V_{in} + V_{out})$$

$$D = \frac{V_{out}}{V_{in} + V_{out}} \quad (25)$$

From equation 25, it is quite clear now that the duty cycle depends on both input and output voltage. Further, it is maximum when the input voltage is lowest, while minimum when the input voltage is highest.

4.2.2 Inductor Value

When the switch will be closed, then the voltage across the inductors L1 and L2 is Vin

$$V_{L1} = V_{in} \quad (26)$$

$$L1 \frac{di_{L1}}{dt} = V_{in}$$

$$\frac{di_{L1}}{dt} = \frac{V_{in}}{L1} = \frac{\Delta i_{L1}}{\mathrm{DT}} = \frac{V_{in}}{L1}$$

$$\Delta i_{L1} = \frac{V_{in}}{L1} DT$$

$$L1 = \frac{V_{in}}{\Delta i_{L1}} DT \quad (27)$$

A similar procedure can be applied to inductor L2

$$L2 = \frac{V_{in}}{\Delta i_{L2}} DT \quad (28)$$

Equations (27) and (28) are used to calculate the value of inductor L1 and inductor L2 for the SEPIC converter.

4.2.3 Capacitor Value

The capacitor is needed to store and smooth the DC voltage [34]. During the selection of the capacitor, the minimum ripple in the output DC voltage must be considered [35]. To accomplish this task we must select a capacitor with low equivalent series resistance, the

Power System Technology
ISSN:1000-3673
Received: 06-06-2024 Revised: 15-07-2024 Accepted: 28-08-2024

voltage rating of the SEPIC capacitor must be greater than the maximum input voltage. As we know:

$$\Delta Q = C\Delta V \tag{29}$$

$$\Delta V = \frac{\Delta Q}{C} \quad where\, \Delta Q = I_{out} DT$$

$$\Delta V = \frac{I_{out} DT}{C} \tag{30}$$

$$C = \frac{I_{out} DT}{\Delta V} \quad since\, I_{out} = \frac{V_{out}}{R}\, and \quad V_{out} = \frac{D}{D'} V_{in}$$

Substitution yields

$$C = \frac{D^2 V_{in} T}{\mathrm{D'R}\Delta V}$$

$$C = \frac{D^2 V_{in}}{\mathrm{D'R}\Delta V f} \tag{31}$$

Where "ΔV" is peak-to-peak ripple voltage by assuming no series equivalent resistance and "f" is the switching frequency. When picking the output capacitor value, the series equivalent resistance must be taken into consideration to ensure the output ripple voltage is inside the required limits.

4.3 The Closed Loop DC-DC SEPIC Converter

In those applications, where the input DC voltage is constant, the basic SEPIC converter given in Figure 10 works fine by applying a pulse train of a constant duty cycle to the gate of the semiconductor switch. But, in those applications, where the input voltage is continuously changing, i.e. the output of a PEH through the bridge rectifier, the output voltage of the SEPIC converter must be continuously monitored and set to the required level by applying a variable duty cycle [36]. The structure of the closed-loop SEPIC converter will look like Figure 14.

Power System Technology
ISSN:1000-3673
Received: 06-06-2024 Revised: 15-07-2024 Accepted: 28-08-2024

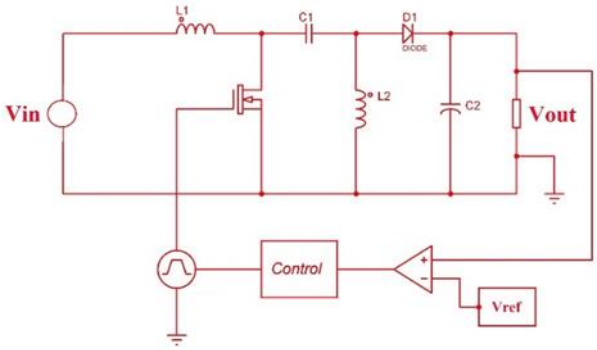

Figure 14 (SEPIC Converter with Feedback)

The output of the SEPIC converter is applied to the load as well as to the non-inverting input of the comparator in a feedback loop. The voltage level required at the output of the SEPIC converter will be applied as the Vref to the inverting input of the same comparator. The output of the comparator will produce the difference voltage between the actual output of the converter and the required value. The output of the comparator has been applied to a controller, which will control the duty cycle of the pulse train applied to switch S1. This duty cycle will be varied until the difference between the output voltage of the converter and the required value becomes zero. Hence, the output of the converter will be a constant voltage irrespective of the changes in input voltage.

5 Simulink Model of the SEPIC converter for Piezoelectric Energy Harvester

In WSN applications, all the motes are operated by 3.3V, so a DC-DC SEPIC converter has been designed to get this voltage from a wide range of voltage coming from the output of the piezoelectric harvester array and bridge rectifier. The array used in this application has energy harvesters in series and parallel combinations, which generate a voltage between 2V and 20V, while the output peak current was 150mA. If more current or voltage is required, then the number of piezoelectric sensors may be increased.

5.1 The complete simulation model

In Figure 15, the complete Simulink model is given, which consists of the piezoelectric harvester, bridge rectifier, improved SEPIC converter with PI type-II controller and scope to display different system parameters. The energy generated by the array of PEHs depends upon the traffic density on the bridge, more traffic means more energy. For this purpose, the Simulink block “signal builder” has been used, which generates different output voltage for different time slots, and depicts the variations in generated energy as per the variable traffic density. Since the output of piezoelectric harvesters is an alternating current (AC) voltage, an

Power System Technology
ISSN:1000-3673
Received: 06-06-2024 Revised: 15-07-2024 Accepted: 28-08-2024

AC voltage generator block is used for this purpose. The variations in the traffic density on the bridge are shown in Figure 15.

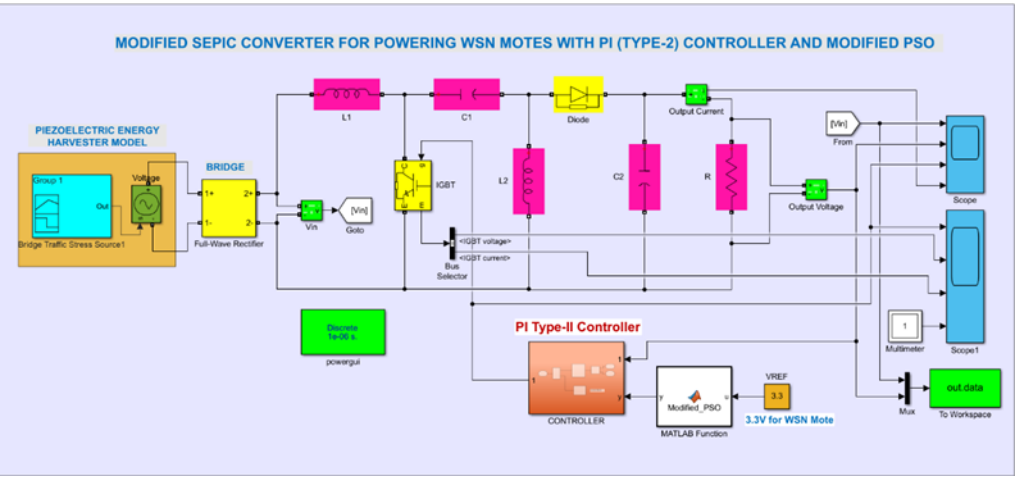

Figure 15 (The complete simulation model)

The designed converter has been tested for a wide range of input voltage, i.e. 6V, 10V, 14V and 18V. For all these mentioned voltages, it provides 3.3VDC.

Table 2 (Values of the SEPIC converter components)

Switching Frequency	F=50kHz
Inductor (L1)	L1=1.56mH
Inductor (L2)	L2=3.24mH
Capacitor (C1)	C1=2.2uF
Capacitor (C1)	C2=C1=2.2uF
Load	RL=50 Ω
Vin	Vin=2V to 20V
Vout	Vout=3.3V
Duty Cycle	Variable (depends upon the Vin)

5.2 The PSO Optimized PI type-II Controller

The SEPIC converter requires a controller to continuously monitor the input voltage coming from the Piezoelectric energy harvester and set the output voltage needed for the WSN motes and charging the batteries. In this regard, an efficient controller is necessary to perform this function. In this design, a PI type-II controller is used, which has been optimized by a modified particle swarm optimization (MPSO) [37] [38]. Figure 16 shows the block diagram of the SEPIC converter with the PI type-II controller with MPSO optimization.

Power System Technology
ISSN:1000-3673
Received: 06-06-2024 Revised: 15-07-2024 Accepted: 28-08-2024

The 'type-II' controller is a kind of lead-type controller with a pole at the origin. Hence, this controller provides a maximum of 90° phase boost with zero steady-state error. Despite having the non-minimum phase problem, the SEPIC converter exhibits a better closed-loop performance with the type-II controller. By proper tuning of the type-II controller using the PSO algorithm, the converter performs a faster response, with nominal overshoots and zero steady-state error [38].

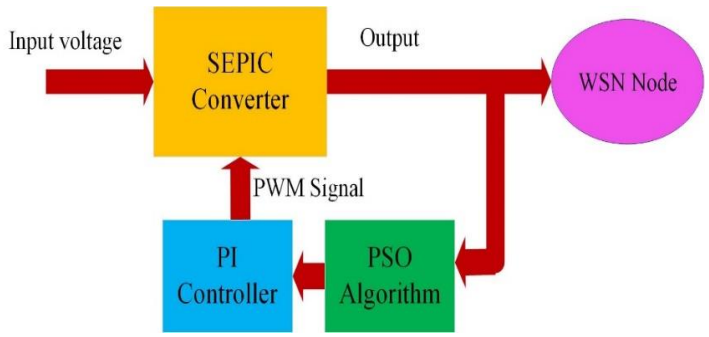

Figure 16 (SEPIC Converter using PI Type-II Controller and optimized by MPSO)

6 Results and Discussion

The designed SEPIC converter characteristics are discussed in this section. The results show, that the designed converter is efficient enough to convert all the voltages coming from the piezoelectric harvester to a constant 3.3VDC required for the WSN motes and battery charging. To evaluate all the possible scenarios, different traffic densities on the bridge have been considered and a Simulink model is designed for generating voltages proportional to the traffic density on the bridge. The converter is tested with a wide range of voltages coming from an array of piezoelectric harvesters depending upon the traffic density on the bridge. Figure 17 presents the varying traffic densities on the bridge in the range of minimum to maximum. Normalized variations in the traffic densities are shown in this figure. At time 0 minutes, the traffic density of vehicles is 40%, similarly, at time 0.2 minutes, it is 60% and so on. These variations in the traffic density will produce proportional voltage at the output of the piezoelectric energy harvester. The AC voltage produced at the energy harvester output is then passed through the rectifier to get DC voltage.

Power System Technology
ISSN:1000-3673
Received: 06-06-2024 Revised: 15-07-2024 Accepted: 28-08-2024

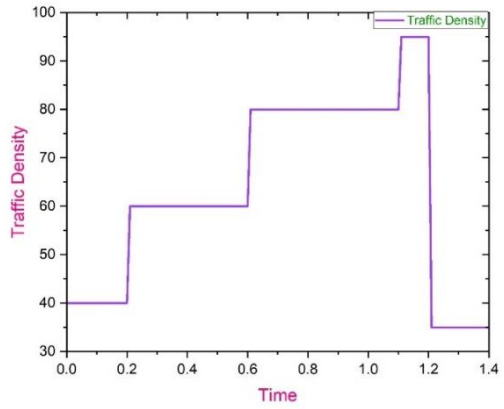

Figure 17 (Normalized variations in traffic density on the bridge)

Figure 18(a) shows the generated voltages at the output of the rectifier. This output signal is proportional to the traffic densities shown in Figure 17. As a result of varying traffic density on the bridge, there are large variations in the output voltage of the energy harvester and sometimes it may be 0V when there is no traffic on the bridge. In this application, the load is a WSN node, which requires a regulated 3.3VDC. So a SEPIC converter has been used to provide fixed 3.3V to the WSN node. It is worth mentioning, that the SEPIC converter is a type of DC-DC converter, which works as both buck and boost converter. This means, that in both cases, it will give 3.3V at output, whether the output voltage of the harvester is less than or greater than 3.3V. The output of the SEPIC converter is shown in Figure 18(b). It is exactly 3,3VDC, except there are small voltage spikes when there is an abrupt change in the traffic density.

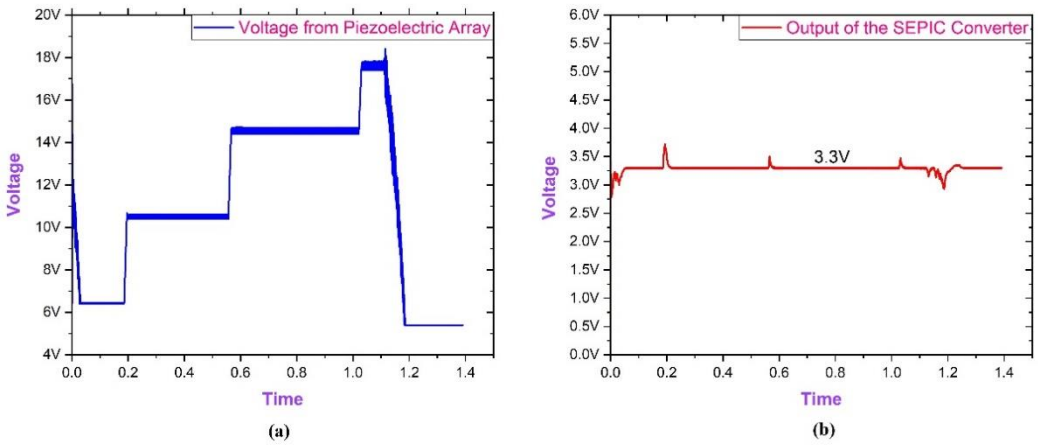

Figure 18 ((a) Voltage from the piezoelectric array (b) Voltage from the SEPIC converter output)

Power System Technology
ISSN:1000-3673
Received: 06-06-2024 Revised: 15-07-2024 Accepted: 28-08-2024

5.3 Response of the converter on fluctuating the input voltage

The designed SEPIC converter characteristics are discussed in this section. The results show, that the converter is efficiently converting the voltage of the piezoelectric harvester with large variations to a fixed 3.3VDC, whether the converter input is increasing or decreasing.

5.3.1 When the voltage of the piezoelectric harvester through the rectifier changes from 8 V to 6 V

In Figure 19(a), the voltage coming from the energy harvester changes from 8V to 6V and the converter is giving fixed 3.3V at output with a minor negative spike. The output is shown in Figure 19(b).

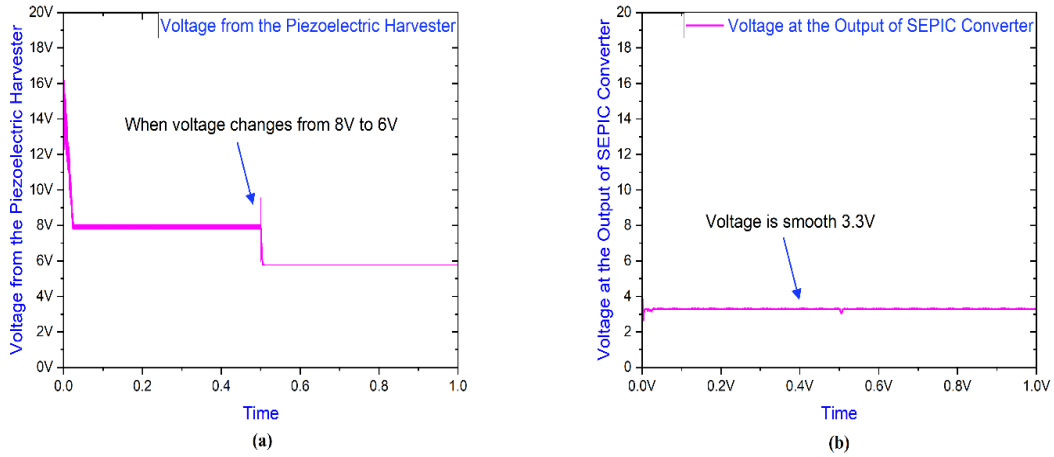

Figure 19 ((a) When voltage changes from 8 V to 6 V (b) Voltage at the output of SEPIC converter)

5.3.2 When the voltage of the piezoelectric harvester through the rectifier changes from 6 V to 3 V

Figure 20(a) presents the harvester output, when the voltage changes from 8V to 6V. Again the converter is giving fixed 3.3V at output with a minor negative spike. The output is shown in Figure 20(b).

Power System Technology
ISSN:1000-3673
Received: 06-06-2024 Revised: 15-07-2024 Accepted: 28-08-2024

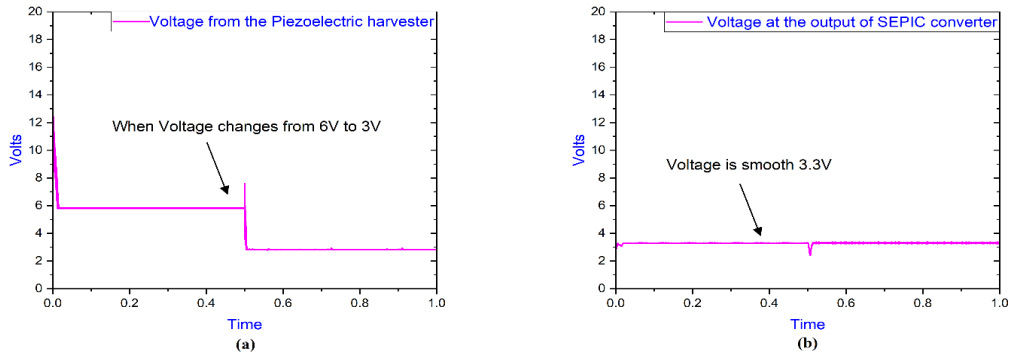

Figure 20 ((a) When voltage changes from 6 V to 3 V (b) Voltage at the output of SEPIC converter)

5.3.3 When the voltage of the piezoelectric harvester through the rectifier changes from 6 V to 11 V

Figure 21(a) shows another large variation in the SEPIC converter's output, which is 6V to 11V. But the converter is efficiently absorbing all the extra voltage and giving fixed 3.3VDC, as shown in Figure 20(b).

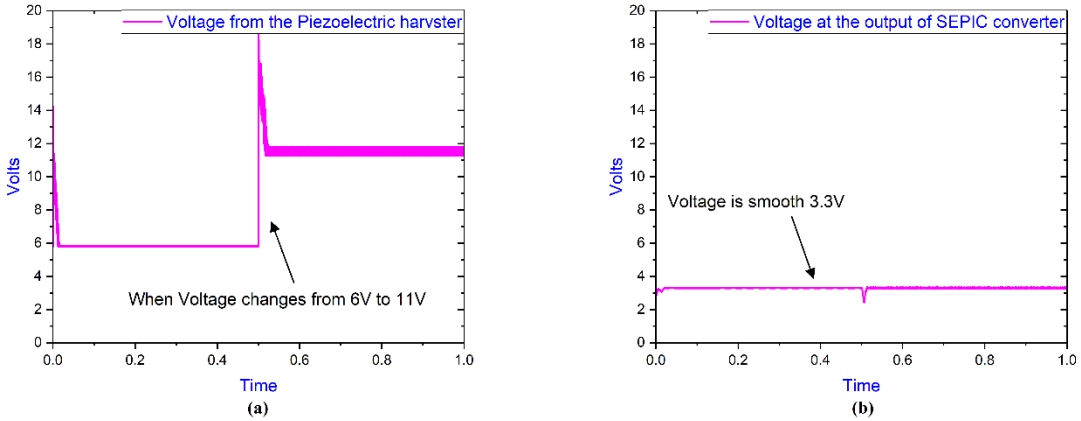

Figure 21 ((a) When voltage changes from 6 V to 11 V (b) Voltage at the output of SEPIC converter)

6 Conclusion

To validate the functionality and performance of the proposed Single-Ended Primary Inductor Converter (SEPIC) converter, a comprehensive model was meticulously developed, rigorously tested, and meticulously simulated within the MATLAB Simulink environment. This model was designed to evaluate the converter's efficiency under various traffic densities on the bridge,

Power System Technology
ISSN:1000-3673
Received: 06-06-2024 Revised: 15-07-2024 Accepted: 28-08-2024

as well as its capability to harness energy from a piezoelectric energy harvester. The MATLAB Simulink simulation demonstrated exceptional performance across the entire spectrum of traffic densities encountered on the bridge, reflecting the versatility and reliability of the SEPIC converter. Even when subjected to scenarios with abrupt changes in voltage levels, the model exhibited remarkable stability, with only negligible voltage spikes detected. This resilience in the face of varying traffic patterns and energy generation profiles underscores the converter's ability to seamlessly adapt to real-world conditions, ensuring a consistent and efficient energy conversion process. In summary, the MATLAB Simulink-based simulation not only confirmed the feasibility of the SEPIC converter but also highlighted its robustness and adaptability in response to dynamic environmental conditions. The converter's capacity to effectively manage and convert energy from the piezoelectric harvester underscores its potential to play a pivotal role in sustainable and self-sufficient energy generation, particularly in applications where capturing and utilizing ambient mechanical energy sources is paramount.

7 **Conflicts of Interest:** The authors declare that they have no known competing financial interests or personal relationships that could have appeared to influence the work reported in this paper.

References

[1] Y. Zhang, W. Zhang, F. Gao, S. Gao, and D. J. Rogers, "A Switched-Capacitor Interleaved Bidirectional Converter with Wide Voltage-Gain Range for Super Capacitors in EVs," *IEEE Trans. Power Electron.*, vol. 35, no. 2, pp. 1536–1547, 2020, doi: 10.1109/TPEL.2019.2921585.

[2] N. Khan, E. Kalair, N. Abas, A. R. Kalair, and A. Kalair, "Energy transition from molecules to atoms and photons," *Eng. Sci. Technol. an Int. J.*, vol. 22, no. 1, pp. 185–214, Feb. 2019, doi: 10.1016/J.JESTCH.2018.05.002.

[3] S. Chakraborty, H. N. Vu, M. M. Hasan, D. D. Tran, M. El Baghdadi, and O. Hegazy, "DC-DC converter topologies for electric vehicles, plug-in hybrid electric vehicles and fast charging stations: State of the art and future trends," *Energies*, vol. 12, no. 8, 2019, doi: 10.3390/en12081569.

[4] J. Joseph, P. R. M. Patel, and H. R. Pathak, "Analysis and Comparison of DC - DC Converter Topologies for the Design and Development of a Solar Based Inverterless System," *Proc. 2nd Int. Conf. Electron. Commun. Aerosp. Technol. ICECA 2018*, pp. 1429–1434, Sep. 2018, doi: 10.1109/ICECA.2018.8474867.

[5] M. Kamran, S. U. Khan, R. Ullah, and S. Akbar, "An FPGA Implementation of PWM for DC-DC SEPIC Converter for Wireless Sensor Network," in *1st International Conference on Electrical, Communication and Computer Engineering, ICECCE 2019*, Jul. 2019. doi: 10.1109/ICECCE47252.2019.8940780.

Power System Technology
ISSN:1000-3673
Received: 06-06-2024 Revised: 15-07-2024 Accepted: 28-08-2024

[6] S. Y. Fadhlullah and W. Ismail, "Solar energy harvesting design framework for 3.3 v small and low-powered devices in wireless sensor network," *2015 Int. Conf. Telemat. Futur. Gener. Networks, TAFGEN 2015*, pp. 89–94, Oct. 2015, doi: 10.1109/TAFGEN.2015.7289583.

[7] I. M. Pop-Calimanu, S. Popescu, and D. Lascu, "A New SEPIC-Based DC-DC Converter with Coupled Inductors Suitable for High Step-Up Applications," *Appl. Sci. 2022, Vol. 12, Page 178*, vol. 12, no. 1, p. 178, Dec. 2021, doi: 10.3390/APP12010178.

[8] C. Covaci and A. Gontean, "Piezoelectric Energy Harvesting Solutions: A Review," *Sensors 2020, Vol. 20, Page 3512*, vol. 20, no. 12, p. 3512, Jun. 2020, doi: 10.3390/S20123512.

[9] M. Abdulkarem, K. Samsudin, F. Z. Rokhani, and M. F. A Rasid, "Wireless sensor network for structural health monitoring: A contemporary review of technologies, challenges, and future direction," *https://doi.org/10.1177/1475921719854528*, vol. 19, no. 3, pp. 693–735, Jul. 2019, doi: 10.1177/1475921719854528.

[10] "Wireless Sensor Networks for Improved Long-Term Bridge Performance | LORD Sensing Systems." https://www.microstrain.com/applications/wireless-sensor-networks-improved-long-term-bridge-performance (accessed Jul. 11, 2021).

[11] M. R. Senouci and A. Mellouk, "Wireless Sensor Networks," *Deploying Wirel. Sens. Networks*, pp. 1–19, 2016, doi: 10.1016/B978-1-78548-099-7.50001-5.

[12] M. Carlos-Mancilla, E. López-Mellado, and M. Siller, "Wireless Sensor Networks Formation: Approaches and Techniques," *J. Sensors*, vol. 2016, pp. 1–18, 2016, doi: 10.1155/2016/2081902.

[13] P. Sengar and N. Bhardwaj, "A Survey on Security and Various Attacks in Wireless Sensor Network," 2017.

[14] A. Dhamgaye and N. Chavhan, "Survey on security challenges in VANET," *Int. J. Comput. Sci. Netw.*, vol. 2, no. No.1, p. 134, 2013.

[15] "Evolution of industrial wireless sensor networks." https://www.eenewseurope.com/design-center/evolution-industrial-wireless-sensor-networks/page/0/1 (accessed Jul. 11, 2021).

[16] B. C. Sekhar *et al.*, "Piezoelectricity and Its Applications," *Multifunct. Ferroelectr. Mater.*, Sep. 2021, doi: 10.5772/INTECHOPEN.96154.

[17] E. Carvalho, L. Fernandes, C. M. Costa, and S. Lanceros-Méndez, "Piezoelectric Polymer Composites for Sensors and Actuators," *Encycl. Mater. Compos.*, pp. 473–486, 2021, doi: 10.1016/B978-0-12-819724-0.00005-7.

[18] M. Smith and S. Kar-Narayan, "Piezoelectric polymers: theory, challenges and opportunities," *https://doi.org/10.1080/09506608.2021.1915935*, vol. 67, no. 1, pp. 65–88, 2021, doi: 10.1080/09506608.2021.1915935.

Power System Technology
ISSN:1000-3673
Received: 06-06-2024 Revised: 15-07-2024 Accepted: 28-08-2024

[19] W. Qian, W. Yang, Y. Zhang, C. R. Bowen, and Y. Yang, "Piezoelectric Materials for Controlling Electro-Chemical Processes," *Nano-Micro Lett. 2020 121*, vol. 12, no. 1, pp. 1–39, Jul. 2020, doi: 10.1007/S40820-020-00489-Z.

[20] H. Mahmoodi Nasrabadi, M. Mahdavi, M. Soleymaniha, and S. O. R. Moheimani, "High resolution atomic force microscopy with an active piezoelectric microcantilever," *Rev. Sci. Instrum.*, vol. 93, no. 7, p. 073706, Jul. 2022, doi: 10.1063/5.0090668.

[21] A. Othman, "Modeling of piezoelectric energy harvesting system embedded in soldier's boot using Matlab/Simulink," *ICMT 2017 - 6th Int. Conf. Mil. Technol.*, pp. 787–792, Jul. 2017, doi: 10.1109/MILTECHS.2017.7988862.

[22] J. Zhao and Z. You, "A Shoe-Embedded Piezoelectric Energy Harvester for Wearable Sensors," *Sensors 2014, Vol. 14, Pages 12497-12510*, vol. 14, no. 7, pp. 12497–12510, Jul. 2014, doi: 10.3390/S140712497.

[23] D. Kumar, P. Chaturvedi, and N. Jejurikar, "Piezoelectric energy harvester design and power conditioning," *2014 IEEE Students' Conf. Electr. Electron. Comput. Sci. SCEECS 2014*, 2014, doi: 10.1109/SCEECS.2014.6804491.

[24] "Piezo Bender Energy Harvester - MATLAB & Simulink." https://www.mathworks.com/help/sps/ug/piezo-bender-energy-harvester.html;jsessionid=bb07be280a228e88d40b4d914538 (accessed Feb. 10, 2023).

[25] H. C. Song, S. W. Kim, H. S. Kim, D. G. Lee, C. Y. Kang, and S. Nahm, "Piezoelectric Energy Harvesting Design Principles for Materials and Structures: Material Figure-of-Merit and Self-Resonance Tuning," *Adv. Mater.*, vol. 32, no. 51, Dec. 2020, doi: 10.1002/ADMA.202002208.

[26] X. Ma *et al.*, "Tuneable resonance frequency vibrational energy harvester with electret-embedded variable capacitor," *IET Nanodielectrics*, vol. 4, no. 2, pp. 53–62, Jun. 2021, doi: 10.1049/NDE2.12007.

[27] W. Zhou *et al.*, "Piezoelectric vibration energy harvester: Operating mode, excitation type and dynamics," *Adv. Mech. Eng.*, vol. 14, no. 10, Oct. 2022, doi: 10.1177/16878132221131177/ASSET/IMAGES/LARGE/10.1177_16878132221131177-FIG2.JPEG.

[28] M. A. Halim, M. Humayun Kabir, H. Cho, and J. Y. Park, "A Frequency Up-Converted Hybrid Energy Harvester Using Transverse Impact-Driven Piezoelectric Bimorph for Human-Limb Motion," *Micromachines 2019, Vol. 10, Page 701*, vol. 10, no. 10, p. 701, Oct. 2019, doi: 10.3390/MI10100701.

[29] Y. Hara *et al.*, "Piezoelectric-silicone structure for vibration energy harvesting: experimental testing and modelling," *Smart Mater. Struct.*, vol. 30, no. 3, p. 035002, Jan. 2021, doi: 10.1088/1361-665X/ABD964.

Power System Technology
ISSN:1000-3673
Received: 06-06-2024 Revised: 15-07-2024 Accepted: 28-08-2024

[30] X. Xu, D. Cao, H. Yang, and M. He, "Application of piezoelectric transducer in energy harvesting in pavement," *Int. J. Pavement Res. Technol.*, vol. 11, no. 4, pp. 388–395, Jul. 2018, doi: 10.1016/J.IJPRT.2017.09.011.

[31] R. Ahmed *et al.*, "A review of energy harvesting using piezoelectric materials: state-of-the-art a decade later (2008–2018)," *Smart Mater. Struct.*, vol. 28, no. 11, p. 113001, Oct. 2019, doi: 10.1088/1361-665X/AB36E4.

[32] M. R. Çorapsız and H. Kahveci, "Performance Analysis of Buck-Boost and SEPIC Converter for Commutation Torque Ripple Minimization in BLDC Motors," *https://doi.org/10.1080/15325008.2022.2049653*, vol. 49, no. 11–12, pp. 1052–1067, 2022, doi: 10.1080/15325008.2022.2049653.

[33] A. Goudarzian, A. Khosravi, and H. Ali Raeisi, "Modeling, design and control of a modified flyback converter with ability of right-half-plane zero alleviation in continuous conduction mode," *Eng. Sci. Technol. an Int. J.*, vol. 26, p. 101007, Feb. 2022, doi: 10.1016/J.JESTCH.2021.05.011.

[34] N. R. Babu and L. C. Saikia, "Optimal location of accurate HVDC and energy storage devices in a deregulated AGC integrated with PWTS considering HPA-ISE as performance index," *Eng. Sci. Technol. an Int. J.*, vol. 33, p. 101072, Sep. 2022, doi: 10.1016/J.JESTCH.2021.10.004.

[35] H. B. Dave, D. Singh, and H. O. Bansal, "Multiple linear regression-based impact analysis of impedance network design on life expectancy of DC-link capacitor in q-ZSI fed motor drive," *Eng. Sci. Technol. an Int. J.*, vol. 24, no. 1, pp. 171–182, Feb. 2021, doi: 10.1016/J.JESTCH.2020.06.004.

[36] C. Vlad, M. A. Bancila, T. Munteanu, and G. Murariu, "Using renewable energy sources for electric vehicles charging," *2013 4th Int. Symp. Electr. Electron. Eng. ISEEE 2013 - Proc.*, no. May 2020, 2013, doi: 10.1109/ISEEE.2013.6674349.

[37] S. Khan, M. Kamran, O. U. Rehman, L. Liu, and S. Yang, "A modified PSO algorithm with dynamic parameters for solving complex engineering design problem," *Int. J. Comput. Math.*, vol. 95, no. 11, pp. 2308–2329, 2018, doi: 10.1080/00207160.2017.1387252.

[38] A. Ghosh, S. Banerjee, M. K. Sarkar, and P. Dutta, "Design and implementation of type-II and type-III controller for DC-DC switched-mode boost converter by using K-factor approach and optimisation techniques," *IET Power Electron.*, vol. 9, no. 5, pp. 938–950, Apr. 2016, doi: 10.1049/IET-PEL.2015.0144.